RESEARCH ARTICLE | JUNE 16 2005

# Deep ultraviolet Raman scattering characterization of ion-implanted SiC crystals

S. Nakashima; T. Mitani; J. Senzaki; H. Okumura; T. Yamamoto



*J. Appl. Phys.* 97, 123507 (2005)
https://doi.org/10.1063/1.1931039

# Deep ultraviolet Raman scattering characterization of ion-implanted SiC crystals

S. Nakashima,[a] T. Mitani, J. Senzaki, and H. Okumura
*National Institute of Advanced Industrial Science and Technology Umezono 1-1-1, Central 2, Tsukuba, Japan*

T. Yamamoto
*Sumitomo Chemical Company Ltd., 6 Kitahara, Tsukuba Ibaraki 300-3294, Japan*

(Received 6 January 2005; accepted 19 April 2005; published online 16 June 2005)

Multiple energy phosphorous ions were implanted into 4H-SiC at room temperature and at an elevated temperature (500 °C) followed by annealing at various temperatures. Deep ultraviolet Raman microscopy was used to analyze the effect of the implantation dose and postannealing temperature on the recovery of surface layers damaged by the implantation. The Raman analysis showed that the recovery rate of the crystallinity increased with an increase in the annealing temperature. However, for highly dosed samples, recovery was not complete even with annealing temperatures up to 1700 °C. With room-temperature implantation, part of the implanted layer was converted into a 3C structure with heavy stacking faults. New Raman bands were observed at below 500 $cm^{-1}$ in samples heavily dosed with $4.0\times10^{16}$ $cm^{-2}$ after annealing, which revealed that excess phosphorus precipitates. A downshift of the phonon Raman bands and a reduction in the LO–TO-phonon frequency splitting were observed in as-implanted samples and ones that are not completely recovered by annealing. This feature is discussed based on several mechanisms. © *2005 American Institute of Physics*. [DOI: 10.1063/1.1931039]

## I. INTRODUCTION

Ion implantation is a key technology for impurity doping in semiconductors. This technology can be used to produce well-defined doping profiles in semiconductor device structures. However, it generates a high density of defects in crystals. High-temperature implantation (hot implantation) followed by high-temperature annealing is required to restore crystallinity and to activate the implanted dopants by replacing them to lattice sites.

Optimization of the ion implantation and annealing processes requires characterization of the physical properties of the implanted region on a microscopic scale. Various techniques including transmission electron microscopy (TEM), electron-transport measurement, and optical spectroscopy have been used for characterizing ion-implanted and postannealed layers. Among the optical techniques, Raman spectroscopy has been actively used to evaluate implantation-induced damages in semiconductors as well as strain and electrical activity of the implanted dopants. This is because the Raman probing depth is comparable to the depth of the implanted layers when a suitable visible laser source is used. Extensive Raman scattering studies have been performed on III-V compounds[1–14] and IV-IV semiconductors including diamond,[15–17] Si,[18–22] and wide gap semiconductors such as SiC (Refs. 23–29) and GaN.[30–32] However, up to now, Raman analysis of the semiconductor surface using visible excitation has been limited to narrow and midgap semiconductors; no systematic studies have been performed on wide gap semiconductors. The main reason for this limitation is that visible light penetrates deeply into wide gap semiconductors, and the strong signals arising from the substrate prevent the observation of signals from thin implanted surface layers. Recent high-speed device fabrication requires shallow junctions, which need implanted layers on a nanometer scale. Nondestructive characterization is obviously needed for such thin layers.

Here we report on the use of Raman microspectroscopy to study phosphorous ion ($P^+$)-implanted 4H-SiC crystals. We used a deep ultraviolet (DUV) laser as an excitation source, whose optical penetration depth is comparable to the implanted layer thickness. Phosphorous implantation has recently attracted much attention because it gives low sheet resistance.[33–37] We used ion-implanted samples with different doping levels ($3.3\times10^{17}$ to $8.0\times10^{20}$ $cm^{-3}$) to analyze the recovery of the crystallinity by postannealing as a function of the annealing temperature. We studied and compared the Raman spectra of samples implanted at room temperature and at 500 °C.

## II. EXPERIMENT

### A. Sample preparation

We used *p*-type epitaxial layers grown on 8°-off 4H-SiC (0001) substrates. The carrier density in the virgin epitaxial layers was $5.0\times10^{15}$ $cm^{-3}$. After a standard RCA cleaning, 10-nm-thick oxide films were grown at 1200 °C in a dry $O_2$ atmosphere. Multiple energy implantation was performed at room temperature and at 500 °C to create a box-shaped profile with a uniform dopant distribution to a depth of 300 nm. The implantation energy was varied from 10 to 280 keV. The total doses were $1.0\times10^{13}$, $9.0\times10^{13}$, $1.0\times10^{15}$, 7.0

[a]Electronic mail: nakashima-s@aist.go.jp

 

$\times 10^{15}$, and $4.0\times10^{16}$ cm$^{-2}$, corresponding to phosphorous atom concentrations of $3.3\times10^{17}$, $3.0\times10^{18}$, $3.3\times10^{19}$, $2.3\times10^{20}$, and $8.0\times10^{20}$ cm$^{-3}$. The postimplantation annealing was carried out after conventional chemical cleaning followed by dipping in dilute HF. The implanted samples were rapidly heated to the annealing temperature within 1 min in an Ar atmosphere. After the annealing, the samples were cooled down to room temperature. These were cooled down to 1000 °C within 1 min from the annealing temperature. The annealing temperature and time were varied between 1200 and 1700 °C, and between 30 s and 30 min, respectively. The free-carrier density in the implanted layers after thermal treatment was estimated from the results of Hall-effect measurement.

### B. DUV Raman measurements

The unpolarized Raman scattering spectra of the implanted samples were recorded at room temperature using a micro-Raman spectrometer recently constructed at our institute. Details of this system are described elsewhere.[38] The spectra were excited with an intracavity frequency-doubled $Ar^+$ laser operated at 244 nm. The laser beam was guided into a microscope and focused through a Cassegrain objective with a numerical aperture of 0.38 and a working distance of 7.3 mm. The power and spot size of the laser beam were 15 mW and $\sim3$ $\mu$m on the sample surface, respectively. The scattered light was collected by the same objective and focused onto the slit of a filter spectrometer with a subtractive double monochromator, and dispersed by a 1.5-m monochromator (Sopra UHRS F1500) with a grating of 2400 grooves/mm. This monochromator can be used for single- and double-pass configurations. The signals were detected by a liquid-nitrogen-cooled charge-coupled device (CCD) detector of an open electrode type. The reciprocal linear dispersions of the spectrometer were 40 and 20 cm$^{-1}$/mm for the single- and double-pass configurations, respectively, which corresponded to 1 and 0.5 cm$^{-1}$/pixel on the CCD. The accuracies of the frequency measurement were $\pm1.0$ and $\pm0.5$ cm$^{-1}$, respectively. The absorption coefficient $\alpha$ of SiC at a 244-nm excitation calculated from optical constants reported elsewhere[39] is $0.5\times10^5$ cm$^{-1}$. Since the Raman scattering was done using a quasibackscattering geometry, the Raman probing depth $[1/(2\alpha)]$ was approximately 100 nm for 4H-SiC, which is comparable to projected range in the present experiment. This ensured that we detected Raman signals from the implanted surface layers alone. We used transverse-optical (TO)- and longitudinal-optical (LO)- or LO-phonon plasmon coupled (LOPC) bands for monitoring the structural disorder and electrical properties, respectively. Because of the resonance Raman effect, 4H-SiC crystals show an intense and narrow folded longitudinal acoustic (FLA) band at 610 cm$^{-1}$ in the DUV region.[38] The FLA mode can also be used as a monitor band for the crystallinity with DUV excitation.

To examine how DUV light probes thin SiC implantation layers, we measured the Raman spectra of a 4H-SiC crystal ion implanted at room temperature and postannealed at 1200 °C using three different laser lines: DUV (244 nm), UV (364 nm), and VIS (488 nm). The dose was $7.0\times10^{15}$ cm$^{-2}$, and the thickness of the implanted layer was 300 nm. As shown in Fig. 1, the DUV Raman spectrum shows broad TO and LO bands, while the VIS and UV spectra show sharp TO and LO bands which arise from the underlying nonimplanted region. The UV excitation was not sufficient for evaluating thin ion-implanted SiC layers with submicron thickness. This demonstrates that the Raman penetration depth of the DUV light is less than the thickness of the implanted layer (300 nm) in SiC and that DUV excitation is well suited for probing submicron ion-implanted regions. On the other hand, for completely amorphized surface layers as implanted with a high dose at room temperature, the Raman spectra obtained with VIS and DUV excitations are almost identical, due to the very shallow penetration depth resulting from the strong absorption in the amorphous region of both VIS and DUV lights. This means that the visible Raman excitation is also useful for almost amorphized SiC layers.

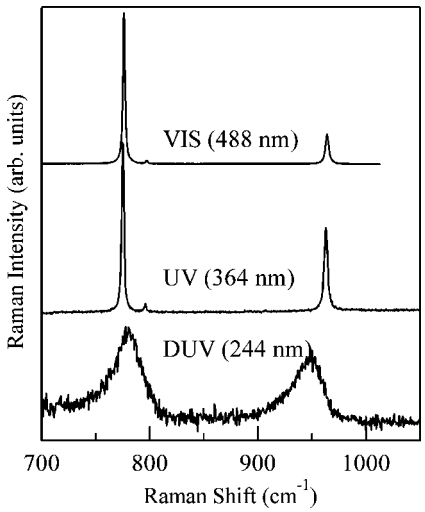


FIG. 1. Raman spectra of 4H-SiC crystals $P^+$ implanted at room temperature with a dose concentration of $2.3\times10^{20}$ cm$^{-3}$ and subsequently annealed at 1200 °C for 30 min. The spectrum measured with DUV (244 nm) excitation is compared with those observed with UV (364 nm) and VIS (488 nm) excitations.

## III. EXPERIMENTAL RESULTS

### A. Hot implantation with low dose

Raman measurements were carried out for phosphorous implanted 4H-SiC crystals with an implant concentration of $3.0\times10^{18}$ cm$^{-3}$. After implantation at 500 °C the samples were annealed at temperatures from 1200 to 1700 °C for 1 min. Figure 2 shows Raman spectra of as-implanted and postannealed samples. The spectrum of a virgin crystal shown for reference exhibits an FLA mode at 610.4 cm$^{-1}$, a folded transverse optical $A_1$ [FTO($A_1$)] mode at 776.4 cm$^{-1}$, and an LO($A_1$) mode at 964.1 cm$^{-1}$.[23] The mode at 784.4 cm$^{-1}$ is a Raman forbidden TO($A_1$) mode, which can be observed at a 244-nm excitation, presumably due to the breakdown of the polarization selection rule under the resonance condition.[38] As shown in this figure, the Raman spectra vary greatly with the annealing temperature. All the Ra-

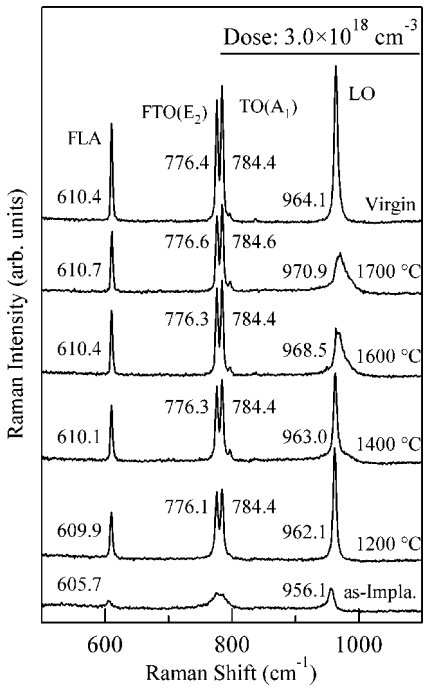


FIG. 2. Raman spectra of 4H-SiC crystals $P^+$ implanted at 500 °C with a dose concentration of $3.0\times10^{18}$ $cm^{-3}$ and subsequently annealed at several temperatures for 1 min.

man bands of the as-implanted sample are markedly broadened. The TO($A_1$) and FTO(2/4) bands merge into a single peak, indicating that the implanted layer is highly damaged but not completely amorphized. As the annealing temperature is increased from 1200 to 1700 °C, these TO bands become sharper and more intense, and are observed separately. The LO band also varies greatly with the annealing temperature.

Figure 3 shows the spectral profiles of the LO bands in Fig. 2 on an expanded scale. At lower-temperature annealing (1200 and 1400 °C) the LO band becomes narrower and stronger. At higher-temperature annealing (1600 and 1700 °C), this band shifts toward the higher-frequency side and takes an asymmetric shape. Such behavior is a characteristic feature of the LO-phonon mode coupled with plasmon.

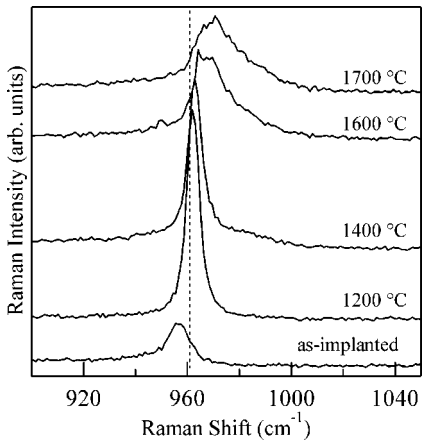


FIG. 3. LO-phonon bands of samples for which spectra are shown in Fig. 2.

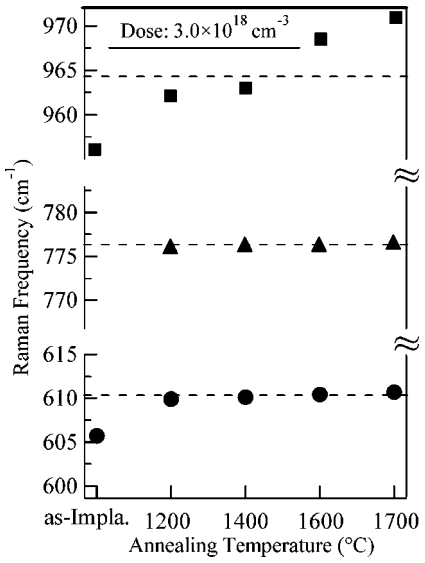


FIG. 4. Peak frequencies of Raman bands of samples for which spectra are shown in Fig. 2, plotted as a function of annealing temperature. The solid circles, triangles, and squares correspond to FLA, FTO ($E_2$), and LO (LOPC) modes, respectively.

The peak frequencies of the FLA, FTO($E_2$), and LO (LOPC) bands are plotted as a function of the annealing temperature in Fig. 4. The FLA and LO bands for the as-implanted sample shift to the low-frequency side. After annealing at temperatures above 1200 °C the FLA and TO bands lie at the same positions as those of the virgin sample. For the annealing at temperatures below 1600 °C, the frequency of the LO band is below that of the pure LO band, though the frequencies of the FLA and TO bands are identical to those of virgin crystal. The LO band shifts to higher frequencies with asymmetric broadening after annealing at 1600 °C. The behavior of the LO mode is explained as follows. With relatively low-temperature annealing (1200 and 1400 °C), the crystallinity partially recovers. However, deep centers resulting in the trapping of free carriers still remain. As a result, annealing at 1200 or 1400 °C yields a sharp symmetric LO band. Annealing at 1600 or 1700 °C increases the free-carrier density due to a reduction of the number of the deep centers and activation of the dopant, resulting in a broad asymmetric LOPC mode shifted to the higher-frequency side, as shown in Fig. 3. The downshift of the LO mode after annealing at 1200 or 1400 °C may be due to a dielectric anomaly, as will be discussed in the next section. For the annealing at 1700 °C, the free-carrier density and electrical activity estimated from the peak frequency of the LOPC mode[28] are about $1.5\times10^{18}$ $cm^{-3}$ and 50%, respectively. The electrical activity of the doping impurity deduced from the Raman analysis is consistent with the result of Hall measurements ($n=1.93\times10^{18}$ $cm^{-3}$).

### B. Room-temperature implantation with high dose

Figure 5 shows the Raman spectra of 4H-SiC implanted at room temperature with a high concentration of phosphorus ($2.3\times10^{20}$ $cm^{-3}$) and subsequently annealed at 1200, 1600, and 1700 °C for 30 min. The as-implanted sample shows no fine structures, indicating that the implanted layer is com-

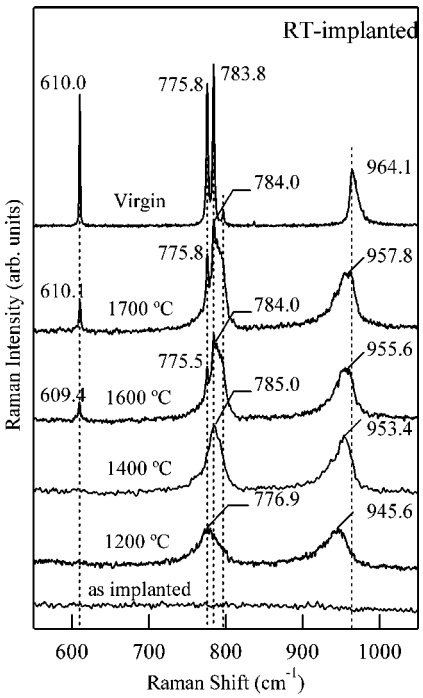


FIG. 5. Raman spectra of 4H-SiC crystals $P^+$ implanted at room temperature with a dose concentration of $2.3\times10^{20}$ cm$^{-3}$. Postannealing temperature ranges from 1200 to 1700 °C. Spectrum of a virgin sample is shown for reference. The annealing time is 30 min.

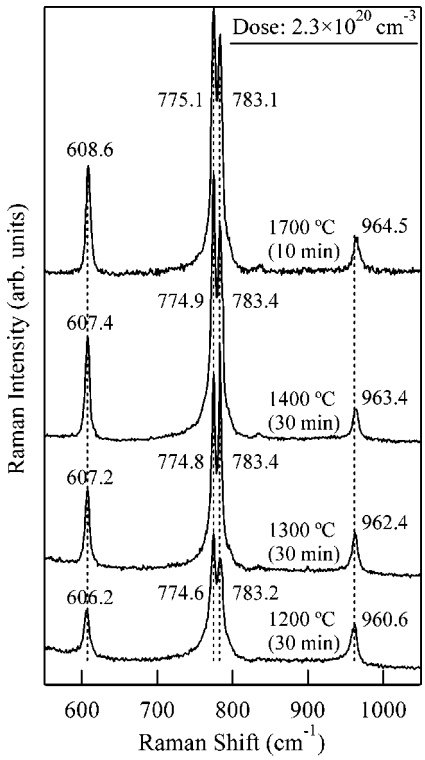


FIG. 6. Raman spectra of 4H-SiC crystals hot implanted with phosphorous ions at 500 °C with a dose concentration of $2.3\times10^{20}$ cm$^{-3}$ and postannealed at several annealing temperatures. The annealing time is shown in this figure for each sample.

pletely amorphized. After annealing at 1200 °C broad TO and LO bands appear. The FLA band at 610 cm$^{-1}$ is absent, and the TO($A_1$) and FTO($E_2$) bands merge into a single band. Furthermore, the TO and LO bands lie at frequencies lower than those of a virgin sample.

For the annealing at 1600 and 1700 °C weak and relatively sharp FLA, FTO($E_2$), and TO($A_1$) bands appear. A broad shoulder band is observed on the higher-frequency side of the TO($A_1$) band extending up to about 795 cm$^{-1}$, corresponding to the frequency of the TO mode of 3C-SiC. This broad asymmetric band is attributed to the TO band of the 3C structure accompanying the high-density stacking faults. The Raman spectra of heavily disordered 3C-SiC have been studied by Rohmfeld *et al.*[40] and Nakashima *et al.*,[41] who showed that a broad band appears below the TO($\Gamma$) band for disordered 3C-SiC. The formation of the 3C stacking in the implanted layer is also supported by the observation that the FLA band at 610 cm$^{-1}$, which is characteristic of 4H-SiC structure, is weak. The presence of weak FTO($E_2$) and TO($A_1$) modes in addition to the weak FLA mode indicates that the implanted layer after annealing consists of heavily disordered 3C structure mixed with a 4H structure. The conversion from implanted $\alpha$-SiC to 3C-SiC by annealing was previously reported by Satoh *et al.*, who showed that 6H-SiC layers implanted at room temperature and postannealed consists of twinned 3C-SiC.[42]

For the implantation at room temperature, the LO-phonon band shows a striking downshift after annealing. For annealing at 1200 °C, the downshift amounts to 18 cm$^{-1}$. For annealing at temperatures from 1400 to 1700 °C, the LO-phonon band is broad and its frequency is 6–9 cm$^{-1}$ lower than that of the virgin crystal. Even after annealing at 1700 °C, the LO-phonon band that accompanies the low-frequency tail is still located at a frequency (957.8 cm$^{-1}$) below that of the pure LO-phonon mode (964 cm$^{-1}$). The downshift of the LO mode shown in Fig. 5 can be attributed to phonon confinement and strain effects, as discussed later. It should be noted that in the present work polytype conversion in the implanted layers was found only for samples implanted at room temperature.

### C. Hot implantation with high dose

Raman measurement was performed on samples $P^+$ implanted at 500 °C with a dose concentration of $2.3\times10^{20}$ cm$^{-3}$. They were postannealed at 1200, 1300, 1400, and 1700 °C for 30 min. The as-implanted sample was almost amorphized. Broad TO and LO bands were observed in the Raman spectrum of the as-implanted sample. As shown in Fig. 6, the intensity of the Raman bands increases gradually with an increase in the annealing temperature. The FTO ($E_2$) and TO($A_1$) bands are not clearly resolved with annealing temperature at 1200 °C, while they are well resolved with annealing at above 1400 °C. After annealing at above 1200 °C, a weak LO band appears at 964 cm$^{-1}$ that corresponds to the pure LO-phonon band in virgin crystal. Hall measurement of these annealed samples indicated that the free-carrier concentration was of the order of $10^{20}$ cm$^{-3}$. For this carrier concentration theoretical analysis of the LOPC mode[28] predicts a very weak and broad LOPC mode beyond 1200 cm$^{-1}$. Accordingly, the appearance of the LO band resembling the bare LO band after postannealing suggests that there are small grains where the free-carrier density is re-

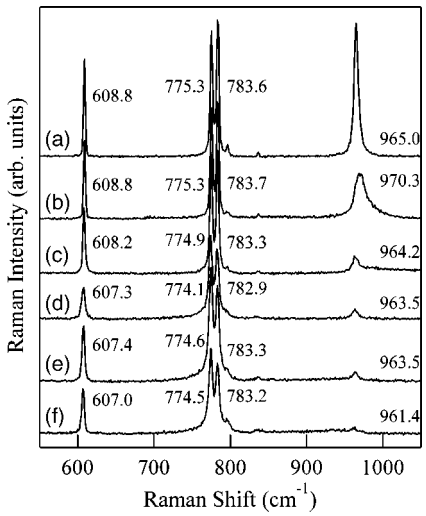


FIG. 7. Raman spectra of 4H-SiC crystals hot implanted with $P^+$ and annealed at 1700 °C. Dose concentrations and annealing times were (a) $3.3\times10^{17}$ cm$^{-3}$, 1 min, (b) $3.0\times10^{18}$ cm$^{-3}$, 1 min, (c) $3.3\times10^{19}$ cm$^{-3}$, 10 min, (d) $2.3\times10^{20}$ cm$^{-3}$, 5 min, (e) $4.0\times10^{20}$ cm$^{-3}$, 5 min, and (f) $8.0\times10^{20}$ cm$^{-3}$, 4 min, 50 s.

duced by carrier trapping resulting from implantation-induced defects. The intensity of the FLA mode is relatively weak for annealing below 1400 °C. Although this band becomes intense with annealing at 1700 °C, the FTA doublet at around 200 cm$^{-1}$ is not clearly resolved. (The spectra of a low-frequency portion are not shown here.) This result indicates that the crystal quality is not completely recovered for a dose concentration of $2.3\times10^{20}$ cm$^{-3}$. On annealing at 1700 °C for 30 min, the spectrum became quite similar to the 4H-SiC spectrum. This was due to the evaporation of the surface layer during annealing, as confirmed by secondary-ion-mass spectrometry (SIMS), whereas for a 10-min annealing the spectral profile resembles that of a sample annealed at 1400 °C. The result of the SIMS measurement showed that the evaporation rate at 1700 °C was roughly 40 nm/10 min when a special covering of the sample surface was not made.

We also observed the Raman spectra of samples implanted with a dose concentration of $2.3\times10^{20}$ cm$^{-3}$ which were postannealed at 1700 °C for the time ranging from 0.5 to 30 min. No appreciable anneal time dependence was observed for these samples. This is consistent with the results of previous sheet resistance measurements for samples annealed for different times.[33]

We studied the dose dependence of Raman spectral profiles in samples implanted at 500 °C and subsequently annealed at 1700 °C for different times. Figure 7 shows results for implantation with implant concentrations of $3.3\times10^{17}$, $3.0\times10^{18}$, $3.3\times10^{19}$, $2.3\times10^{20}$, $4.0\times10^{20}$, and $8.0\times10^{20}$ cm$^{-3}$. As the implanted dose is increased, the intensity of the LO band relative to that of the FLA band decreases, and the resolution of the FTO($E_2$) and TO($A_1$) bands slightly worsens owing to the broadening of these Raman bands. This implies that crystal quality with a lower dose after annealing at 1700 °C is better than with a higher dose. The LO band in the sample with a low implant concentration of $3.0\times10^{17}$ cm$^{-3}$ is intense and sharp. For an implant concentration of $3.0\times10^{18}$ cm$^{-3}$, the LOPC mode shifts by $\sim$6 cm$^{-1}$ to the high-frequency side of the bare LO mode. On the contrary, for implant concentrations higher than $3.3\times10^{19}$ cm$^{-3}$ the weak LO mode appears close to or at the lower-frequency side of the bare LO mode. The LOPC mode of the samples with implant concentrations higher than $3.3\times10^{19}$ cm$^{-3}$ should be upshifted, weak, and broadened, because the carrier density is high ($1.4\times10^{19}$–$2.7\times10^{20}$ cm$^{-3}$), as evidenced by Hall measurement. The appearance of a sharp LO mode resembling a bare LO mode indicates the presence of minute clusters with a low carrier density in the implanted layer. The carrier density reduction might be caused by residual defects existing in the clusters. It will be informative to discuss the behavior of as-implanted samples used in this figure. Raman spectra of the as-implanted specimens showed that as the implantation dose is increased, the area of damaged regions increases. For a dose of $3.3\times10^{17}$ cm$^{-3}$ the Raman spectrum of the as-implanted specimen similar to that of pristine crystals. For doses of $3.0\times10^{18}$, $3.3\times10^{19}$, and $2.3\times10^{20}$ cm$^{-3}$ broad and weak Raman bands were observed at positions of the TO and LO modes, indicating that the as-implanted region was almost amorphized. For heavily dosed specimens with $4.0\times10^{20}$ and $8.0\times10^{20}$ cm$^{-3}$ the Raman spectra were featureless, as shown in Fig. 8.

Raman measurement was carried out on 4H-SiC crystals heavily implanted with a dose concentration of $8.0\times10^{20}$ cm$^{-3}$ followed by annealing at 1700 °C for different annealing times. The thickness of the implanted layer was 500 nm. As shown in Fig. 8, the as-implanted sample shows the weak LO and TO bands, and the FLA band disappears,

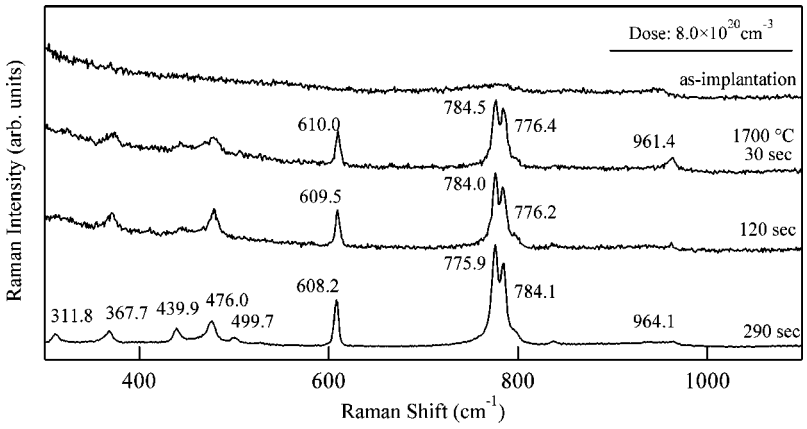


FIG. 8. Raman spectra of 4H-crystals with a heavy dose concentration of $8.0\times10^{20}$ cm$^{-3}$ and short postannealing times.

indicating that the implanted layer is almost amorphized. The FLA, TO ($A_1$), and FTO ($E_2$) bands become narrower as the annealing time is increased. The LO band remains weak and is located near the bare LO band. Hall measurement shows that the carrier density in the implanted layer is as high as $2.7\times10^{20}$ cm$^{-3}$ after annealing for longer than 30 s. As predicted from the behavior of the LOPC mode,[28] this mode should shift towards much higher frequencies in an asymmetric broad band shape. Moreover, the intensity of the LOPC mode should be too weak to be observed for such a high density of free carriers. Hence, the weak LO band observed at around 965 cm$^{-1}$ would arise from clusters where the free-carrier density is greatly reduced due to trapping by residual defects.

The spectra shown in Fig. 8 have a fine structure in the frequency region below 500 cm$^{-1}$. The bands in this structure become sharper as the annealing time is increased. Furthermore, they also appear in samples implanted with a high concentration ($4.0\times10^{20}$ cm$^{-3}$). We attribute these bands to phonon bands in clusters of precipitated phosphorus. Raman measurements have been made on black phosphorus[43] or amorphous phosphorus.[44] Sugai *et al.* observed four strong Raman bands at 194, 362, 439, and 467 cm$^{-1}$ for orthorhombic black phosphorus, which were assigned as $B_{1g}$, $A_g$, $B_{2g}$, and $A_g$ modes, respectively. The peak frequencies of these new Raman bands are close to those reported for the orthorhombic phosphorus, though the bands observed at 367.7 and 476.0 cm$^{-1}$ are by several wave numbers different from the corresponding bands reported by Sugai *et al.*[43] The presence of the unidentified Raman bands at 311.8 and 499.7 cm$^{-1}$ suggests that different P allotropes are mixed in the precipitates. The Raman spectral profile of the phosphorous clusters in Fig. 8 is much different from that of the amorphous phosphorus reported by Olego *et al.*[44] These results indicate that the phosphorous clusters in the implanted layers consist mainly of crystalline orthorhombic phosphorus.

The solubility limit of phosphorus in 4H-SiC has recently been reexamined by Bockstedte *et al.*[45] and Laube *et al.*,[46] who suggested that the upper limit of the solubility for phosphorus is above $10^{20}$ cm$^{-3}$. Phosphorous activation up to $2.7\times10^{20}$ cm$^{-3}$ was achieved with a postimplantation annealing by Negoro *et al.*[34] A high carrier concentration of $3.0\times10^{20}$ cm$^{-3}$ was obtained in heavily dosed 4H-SiC using XeCl laser annealing.[47] As stated above, Hall measurements made on a sample implanted with a dose concentration of $8.0\times10^{20}$ cm$^{-3}$ showed that the electrical activity of the dose impurity was about 30% (the free-carrier concentration was $2.7\times10^{20}$ cm$^{-3}$). Our finding of phosphorous precipitates in samples implanted with a dose concentration of $4.0\times10^{20}$ or $8.0\times10^{20}$ cm$^{-3}$ is consistent with recent studies of the solubility limit of P and our Hall measurements. Recently, precipitation of boron has been observed for 6H-SiC implanted with a boron concentration of $1.5\times10^{21}$ cm$^{-3}$.[48] Precipitates of phosphorus were also found in implanted InP for which a new Raman band has been observed at around 436 cm$^{-1}$.[49]

## IV. DISCUSSION

Our Raman measurements of ion-implanted and postannealed 4H-SiC showed that Raman spectral profiles vary drastically with the dose and annealing conditions. Particular features are a change in the peak frequency and band shape. The downshift of the LO-phonon band has been frequently observed in surface layers of various semiconductors which are ion implanted and also postannealed.[1,4,6–8,50–55] There are several causes for the shift of the phonon Raman bands relative to those of perfect crystals: (i) strain, (ii) phonon confinement, (iii) defect or impurity-induced change in the force constants, and (iv) defect-induced change in the long-range polarization field. Analysis of the frequency shift together with the line shape is an effective way to identify the cause of the downshift in implanted and postannealed materials.

### A. Ion implantation-induced strain

Lattice strain is induced in various materials by ion implantation.[7,8,51,52] The strain may arise from vacancy clusters, interstitials, dislocation loops, stacking faults, etc. We used the frequency shift of phonon bands as a measure of the recovery of the crystallinity. The strain and the change in force constants would tend to cause almost equal shifts for TO and LO mode frequencies. Most of our SiC samples as implanted and postannealed at relatively low temperatures below 1600 °C showed a downshift of the TO and LO-phonon bands. As shown in Figs. 2 and 4, the FLA and LO bands in the as-implanted sample with an implant concentration of $3.0\times10^{18}$ cm$^{-3}$ shift down by 3 and 7 cm$^{-1}$, respectively, from those of virgin crystal. On annealing above 1200 °C the FLA and TO bands return to their original positions. In contrast, the LO band remains downshifted after annealing at 1200 or 1400 °C. This implies that strain mainly contributes to the downshift of the TO and LO bands in the above as-implanted samples, but diminishes after annealing at above 1200 °C.

A downshift of both the TO and LO modes is also observed in the samples hot implanted with a dose concentration of $2.3\times10^{20}$ cm$^{-3}$ and postannealed at below 1400 °C (Fig. 6). As shown in Fig. 6, the FLA and LO-phonon bands shift almost equally to the lower-frequency side with annealing at 1200 °C. We attribute this to implantation-induced strain. Similar features are observed in samples implanted with higher concentrations ($2.3\times10^{20}$ and $1.3\times10^{21}$ cm$^{-3}$) and postannealed at 1700 °C for 1 min (Fig. 7). These results show that the strain tends to remain in SiC crystals that are as implanted and postannealed at lower temperatures. The strain may be relaxed by annealing at temperatures higher than 1700 °C.

### B. Phonon confinement effect and change in dielectric properties

In an imperfect crystal, phonons can be confined in space by microcrystallite boundaries or defects. This confinement results in uncertainty in the phonon momentum and in the wave-vector selection rule during Raman scattering. This allows phonons with $q>0$ to contribute to the Raman scattering, where $q$ is the wave vector of the phonon. Since

the phonon dispersions at the Γ point are negative in general, phonons with frequencies lower than that at the Γ point participate into the Raman scattering. This shifts the Raman peak downward and makes the line shape asymmetric with a low-frequency tail in solids damaged by ion implantation.[1,4,53–55] This phonon confinement effect would affect both LO and TO modes. The amount of the shift may differ a bit between the LO and TO modes because the phonon dispersions for these modes differ.

When the downshift of the LO-phonon band is large compared to that of the TO phonon, or the LO mode alone downshifts, the frequency splitting between the LO and TO mode is reduced. As stated above, the strain and change in force constants usually cause an almost equal shift for the TO and LO mode frequencies. This means that the reduction in the LO–TO splitting would not be due to stress. This reduction has been found in ion-implanted semiconductors,[6,50,56] low-temperature (LT) grown GaAs, GaP[3,6,8,57–59] nitrided GaAs,[60] neutron-irradiated GaP,[6] and ZnO films.[61] A reduction in the LO–TO splitting in ion-implanted GaP has been reported by Myers *et al.*[8] and Kuriyama *et al.*[6] Myers *et al.* interpreted the reduction in the LO–TO splitting in terms of defect-induced weakening of the long-range Coulomb field, which causes a larger downshift for the LO mode than the TO mode. An alternate interpretation is a change in the effective charge due to defects. LT-GaAs and LT-GaP epitaxial films that have excess V group elements[57–59] exhibit reduced LO–TO splitting of the order of 0.5–2.2 $cm^{-1}$. In a dielectric continuum model, the frequencies of the LO and TO modes are related by the equation $\omega_L{}^2-\omega_T{}^2=4\pi Q^2/(\mu\nu\varepsilon_\infty)$, where $\omega_L$ and $\omega_T$ are the LO- and TO-phonon frequencies, $Q$ is the effective charge on the ions, $\nu$ and $\mu$ are the volume and reduced mass of the unit cell, and $\varepsilon_\infty$ is the high-frequency dielectric constant.[50] The reduction of the LO–TO splitting has been explained in terms of the reduction in the effective charge caused by antisite defects[50,57,58] and vacancy-interstitial complexes.[50,56,60] Ashkenov *et al.* observed a slight redshift of the LO mode in ZnO film grown on sapphire.[61] They showed that the density of this film is low compared with that of bulk crystal and that the static dielectric constant $\varepsilon_0$ is smaller than that of bulk crystal. They attributed these features to a high density of vacancy point defects. They postulated that vacancies reduce the LO-phonon frequency, which is related to the TO mode frequency via the Lyddane–Sachs–Teller relation due to a decrease in $\varepsilon_0$. While these two explanations for the change in the dielectric property seem to be based on different models, they have one concept in common: *the change in the polarization field due to defects*.

As shown in Figs. 3 and 4, a noticeable downshift of the LO band is observed for SiC samples implanted with a dose concentration of $3.0\times10^{18}$ $cm^{-3}$ and postannealed at 1200 or 1400 °C. The downshift of the LO mode may cause the reduction in the LO–TO splitting. In this case, the LO-phonon band is sharp and almost symmetric. Samples implanted with $8.0\times10^{20}$ $cm^{-3}$ and postannealed at 1700 °C shows a larger downshift of the LO band than of the FLA band [curve (f) in Fig. 7]. This downshift of the LO band is attributed to a decrease in the polarization field caused by implantation-induced defects, since the low-frequency tail of the LO band related to the phonon confinement effect is not observed.

As shown in Fig. 5, there is the remarkable downshift of the LO mode together with a broadening in the lower-frequency side for the samples implanted at room temperature. The peak frequency of the TO bands could not be determined due to their complicated structure. A plausible explanation for the downshift of the LO band is that the LO phonons are confined in the domains of the 3C structure with heavy stacking faults in which the free-carrier density is low. A dielectric anomaly may contribute to the downshift of the LO band in the 3C domains.

It is worth noting that the downshift of phonon band observed in the as-implanted and postannealed SiC cannot always be attributed to a single mechanism. It originates from a mixture of mechanisms such as strain, phonon confinement, and change in dielectric properties; the extent of their contributions depends on the implantation and postannealing conditions.

## V. SUMMARY

We used DUV Raman spectroscopy to study the recovery of crystallinity of 4H-SiC surface layers implanted with phosphorous ions and subsequently annealed. Characterization of the residual strain, recovery of crystallinity, and also electrical properties of the samples postannealed at different temperatures reveals that the recovery of crystallinity depends strongly on implant concentration of phosphorus and the annealing conditions. For samples with low implant concentrations (less than $3.3\times10^{18}$ $cm^{-3}$), the crystallinity is fairly sufficiently recovered after postannealing at 1700 °C. For samples implanted with $\sim2.0\times10^{20}$ $cm^{-3}$ the crystal quality is not fully recovered even after annealing at 1700 °C. The Raman spectra show that the phosphorous ions are segregated in heavily implanted samples ($8.0\times10^{20}$ $cm^{-3}$); this is because the density of the implanted ions exceeded the solubility limit. For samples implanted at room temperature with $2.3\times10^{20}$ $cm^{-3}$, the spectra show that the implanted layers are partly transformed into a 3C stacking structure with heavy stacking faults. The Raman bands for samples as implanted and annealed at lower temperatures are downshifted due to implantation-induced strain, phonon confinement, and changes in the dielectric parameters.

The results of the present work demonstrate that the deep ultraviolet Raman spectroscopy is a powerful technique for characterizing not only the residual strain in thin SiC surface layers but also the recovery of crystallinity by post ion implantation annealing.

## ACKNOWLEDGMENTS

We are grateful to M. Itoh for her help with the Raman measurements. This work is partly supported by the Regional Research and Development Consortium, METI.

[1] K. K. Tiong, P. M. Amirtharaj, F. H. Pollak, and D. E. Aspnes, Appl. Phys. Lett. **44**, 122 (1984).
[2] M. Gargouri, B. Prevot, and C. Schwab, J. Appl. Phys. **62**, 3902 (1987).
[3] M. Holtz, R. Zallen, and O. Brafman, Phys. Rev. B **38**, 6097 (1988).

[4]U. V. Desnica, I. D. Desnica-Franković, M. Ivanda, K. Furić, and T. E. Haynes, Phys. Rev. B **55**, 16205 (1997).
[5]P. Murugan, R. Kesavamoorthy, S. Amirthapandian, R. Saravanan, K. Ramachandran, and N. Krishnamurthy, Physica B **315**, 56 (2002).
[6]K. Kuriyama, T. Kato, S. Tajima, T. Kato, and S. Takeda, Appl. Phys. Lett. **66**, 2995 (1995).
[7]A. Sarua, G. Irmer, J. Monecke, I. M. Tiginyanu, C. Schwab, J.-J. Grob, and H. L. Hartnagel, J. Appl. Phys. **88**, 7006 (2000).
[8]D. R. Myers, P. L. Gourley, and P. S. Peercy, J. Appl. Phys. **54**, 5032 (1983).
[9]L. L. Abels, S. Sundaram, R. L. Schmidt, and J. Comas, Appl. Surf. Sci. **9**, 2 (1981).
[10]B.-R. Shi, N. Cue, T.-B. Xu, and S. Au, J. Appl. Phys. **80**, 2127 (1996).
[11]H. Katsumata, S. Uekusa, H. Sai, and M. Kumagai, J. Appl. Phys. **80**, 2383 (1996).
[12]L. Artús, R. Cuscó, J. Ibáñez, J. M. Martin, and G. González-Días, J. Appl. Phys. **82**, 3736 (1997).
[13]N. Dharmarasu, B. Sundarakkannan, R. Kesavamoorthy, K. G. M. Nair, and J. Kumar, Physica B **262**, 329 (1999).
[14]J. Ibáñez, R. Cuscó, L. Artús, G. Gonzáles-Díaz, and J. Jiménez, Solid State Commun. **121**, 609 (2002).
[15]R. Kalish, A. Reznik, S. Prawer, D. Saada, and J. Adler, Phys. Status Solidi A **174**, 83 (1999).
[16]E. H. Lee, D. M. Hembree, Jr., G. R. Rao, and L. K. Mansur, Phys. Rev. B **48**, 15540 (1993).
[17]J. D. Hunn, S. P. Winthrow, C. W. White, and D. M. Hembree, Jr., Phys. Rev. B **52**, 8106 (1995).
[18]D. Kirillov, R. A. Powell, and D. T. Hodul, J. Appl. Phys. **58**, 2174 (1985).
[19]P. X. Zhang, I. V. Mitchel, P. J. Schultz, and D. J. Lockwood, J. Raman Spectrosc. **25**, 515 (1994).
[20]A. Othonos, C. Christofides, J. Boussey-Said, and M. Bisson, J. Appl. Phys. **75**, 8032 (1994).
[21]T. Motooka and O. W. Holland, Appl. Phys. Lett. **61**, 3005 (1992).
[22]K. Mizoguchi, S. Nakashima, A. Fujii, A. Mitsuishi, H. Morimoto, H. Onoda, and T. Kato, Jpn. J. Appl. Phys., Part 1 **26**, 903 (1987).
[23]J. Camassel, S. Blanque, N. Mestres, P. Godignon, and J. Pascual, Phys. Status Solidi C, **0**, 875 (2003).
[24]R. Héliou, J. L. Berbner, and S. Roorda, Semicond. Sci. Technol. **16**, 836 (2001).
[25]E. Valcheva, T. Paskova, I. G. Ivanov, R. Yakimova, Q. Wahab, S. Savage, N. Nordell, and C. I. Harris, J. Vac. Sci. Technol. B **17**, 1040 (1999).
[26]Z. C. Feng, S. J. Chua, K. Tone, and J. H. Zhao, Appl. Phys. Lett. **75**, 472 (1999).
[27]J. Pezoldt, R. A. Yankov, T. Werninghaus, D. R. T. Zahn, W. Fukarek, G. Teichert, M. Luebbe, and W. Skorupa, Diamond Relat. Mater. **8**, 346 (1999).
[28]S. Nakashima and H. Harima, Phys. Status Solidi A **162**, 39 (1997).
[29]T. Kimoto, A. Itoh, H. Matsunami, T. Nakata, and M. Watanabe, J. Electron. Mater. **24**, 235 (1995).
[30]W. Limmer, W. Ritter, R. Sauer, B. Mensching, C. Liu, and B. Rauschenbach, Appl. Phys. Lett. **72**, 2589 (1998).
[31]M. Katsikini, K. Papagelis, E. C. Paloura, and S. Ves, J. Appl. Phys. **94**, 4389 (2003).
[32]B. Boudart, Y. Guhel, J. C. Pesant, P. Dhamelincourt, and M. A. Poisson, J. Phys.: Condens. Matter **16**, S49 (2004).
[33]J. Senzaki, K. Fukuda, and K. Arai, J. Appl. Phys. **94**, 2942 (2003).
[34]Y. Negoro, K. Katsumoto, T. Kimoto, and H. Matsunami, J. Appl. Phys. **96**, 224 (2004).
[35]M. V. Rao, J. Tucker, O. W. Holland, N. Papanicolaou, P. H. Chi, J. W. Kretchmer, and M. Chezzo, J. Electron. Mater. **28**, 334 (1999).
[36]T. Ohshima, K. Abe, H. Itoh, M. Yoshikawa, K. Kojima, I. Nashiyama, and S. Okada, Appl. Phys. A: Mater. Sci. Process. **71**, 141 (2000).
[37]S. Harada and T. Motooka, J. Appl. Phys. **87**, 2655 (2000).
[38]S. Nakashima, H. Okumura, T. Yamamoto, and R. Shimidzu, Appl. Spectrosc. **58**, 224 (2004).
[39]S. Zollner, J. G. Chen, E. Duda, T. Wetteroth, S. R. Wilson, and J. N. Hilfiker, J. Appl. Phys. **85**, 8353 (1999).
[40]S. Rohmfeld, M. Hundhausen, and L. Ley, Phys. Status Solidi B **215**, 115 (1999).
[41]S. Nakashima, Y. Nakatake, Y. Ishida, T. Takahashiand, and H. Okumura, Physica B **308–310**, 684 (2001).
[42]M. Satoh, Mater. Sci. Forum **389–393**, 773 (2002).
[43]S. Sugai, T. Ueda, and K. Murase, J. Phys. Soc. Jpn. **50**, 3356 (1981).
[44]D. J. Olego, J. A. Baumann, M. A. Kuck, R. Schachter, C. G. Michel, and P. M. Raccah, Solid State Commun. **52**, 311 (1984).
[45]M. Bockstedte, A. Mattausch, and O. Pankratov, Mater. Sci. Forum **457–460**, 715 (2004).
[46]M. Laube, F. Schmid, G. Pensl, G. Wagner, M. Linnarsson, and M. Maier, J. Appl. Phys. **92**, 549 (2002).
[47]Y. Tanaka, H. Tanoue, and K. Arai, Mater. Sci. Forum **389–393**, 799 (2002).
[48]D. Panknin, H. Wirth, A. Mücklich, and W. Skorupa, J. Appl. Phys. **89**, 3162 (2001).
[49]R. Cuscó, G. Talamàs, L. Artús, J. M. Martin, and G. González-Días, J. Appl. Phys. **79**, 3927 (1996).
[50]G. Burns, F. H. Dacol, C. R. Wie, E. Burstein, and M. Cardona, Solid State Commun. **62**, 449 (1987).
[51]R. E. Whan and G. W. Arnold, Appl. Phys. Lett. **17**, 378 (1970).
[52]C. A. Cima, H. Boudinov, J. P. de Souza, Yu. Suprun-Belevich, and P. F. P. Fitchtner, J. Appl. Phys. **88**, 1771 (2000).
[53]S. J. Yu, H. Asahi, S. Emura, H. Sumida, S. Gonda, and H. Tanoue, J. Appl. Phys. **66**, 856 (1989).
[54]G. Braunstein, D. Tuschel, S. Chen, and S-T. Lee, J. Appl. Phys. **66**, 3515 (1989).
[55]O. Brafman and R. Manor, Phys. Rev. B **51**, 6940 (1995).
[56]K. Kuriyama, Y. Miyamoto, and M. Okada, J. Appl. Phys. **85**, 3499 (1999).
[57]T. A. Gant, H. Shen, R. Fremish, L. Fotiadis, and M. Dutta, Appl. Phys. Lett. **60**, 1453 (1992).
[58]Y. He, N. A. El-Masry, J. Ramdani, S. M. Bedair, T. L. McCormick, R. J. Nemanich, and E. R. Weber, Appl. Phys. Lett. **65**, 1671 (1994).
[59]W. C. Lee, T. M. Hsu, J. -I. Chyi, G. S. Lee, W. -H. Li, and K. C. Lee, Appl. Surf. Sci. **92**, 66 (1996).
[60]E. K. Koh, Y. J. Park, E. K. kim, S. K. Min, and S. H. Choh, Phys. Rev. B **57**, 11919 (1998).
[61]N. Ashkeno *et al.*, J. Appl. Phys. **93**, 126 (2003).